

Universality of Shell Effects in Fusion-Fission Mass Distributions

J. Buete^{a,*}, B. M. A. Swinton-Bland^{a,3}, D. J. Hinde^a, K. J. Cook^{a,b}, M. Dasgupta^a, A. C. Berriman^a, D. Y. Jeung^a, K. Banerjee^{a,1}, L. T. Bezzina^a, I. P. Carter^a, C. Sengupta^{a,2}, C. Simenel^{a,c}, E. C. Simpson^a

^aDepartment of Nuclear Physics and Accelerator Applications, Research School of Physics, Australian National University, Canberra, ACT 2601, Australia

^bFacility for Rare Isotope Beams, Michigan State University, Michigan 48824, USA

^cDepartment of Fundamental and Theoretical Physics, Research School of Physics, Australian National University, Canberra, ACT 2601, Australia

Abstract

We present the results of a broad, systematic study of heavy-ion induced fission mass distributions for every even- Z compound nucleus (Z_{CN}) from ^{144}Gd to ^{212}Th . We find systematic evidence of shell-driven structure in *every* fission mass distribution. The change in shape of the mass distributions with Z_{CN} is consistent with the results of quantitative simultaneous fitting in mass and total kinetic energy, demonstrating that fragment proton shell gaps at $Z_{\text{FF}} = 34, 36$ and $Z_{\text{FF}} = 44, 46$ are *both* major drivers of fission mass distributions below the actinide region. The mass distributions show enhanced yields at mass symmetry for values of Z_{CN} equal to two times these favoured Z_{FF} values. Thus, the same shell gaps that are drivers of mass-asymmetric fission also affect mass distributions at and near mass-symmetry. For all systems a second, more mass-asymmetric, fission mode is required to fit the fission mass distributions. If driven by a single shell gap, it appears to be in the light fragment around $Z_{\text{FF}} = 28, 30$.

Keywords: heavy-ion induced fission, fission, nuclear reactions, fission mass distributions, sub-lead fission, shell-driven fission

1. Introduction

Reaching a fundamental understanding of nuclear fission – the division of a single nucleus into two fragments – is one of the grand challenges of nuclear physics. Mass-asymmetric fission has been observed since the discovery of fission [1], where low-energy fission of actinide nuclei shows clear peaks in yield away from mass symmetry. This is contrary to expectations from the liquid-drop description of fission, and is associated with the influence of microscopic degrees of freedom – the influence of the quantum-mechanical level structure of the nascent fission fragments on the potential energy surface (PES).

The mass-asymmetric fission of actinide nuclei is generally interpreted as comprising two main modes, having heavy fragment masses (A_{FF}) centred near 132 and 140. These have been termed the Standard I and Standard II fission modes respectively [2]. Experimental identification of the proton number of the fission fragments (Z_{FF}) revealed that the Standard I and II fission modes are most strongly correlated with the *proton* number of the heavy fragments, being centred near $Z_{\text{FF}} = 52.5$ and 55 [3, 4]. Microscopic calculations find the emergence of shell gaps in octupole-deformed nuclei with $Z_{\text{FF}} = 52$ and 56: shapes expected to be important as the system approaches scission [5].

The observation of dominant mass-asymmetric fission of ^{180}Hg populated at low excitation energy (E^*) following β -decay of ^{180}Tl was the first indication that structure effects can significantly influence fission of nuclides well-below lead [6]. The extracted fission mass distribution showed peaks at fragment masses $A_{\text{FF}} = 80$ and 100. This observation has been associated with proton numbers $Z_{\text{FF}} = 36$ and/or 44 [6], very different from the proton numbers associated with mass-asymmetric fission of the actinides.

Measurements of fission mass distributions of nuclides in the mercury region populated by heavy-ion fusion demonstrated evidence of mass-asymmetric fission persisting [7, 8] at these much higher excitation energies, despite the expected attenuation of shell effects with E^* . Heavy-ion fusion-fission provides access to a wider range of nuclides than β -delayed fission, thus opening up investigation of fission for a wide range of sub-lead nuclei. Subsequent studies of fission from ^{176}Os to ^{209}Bi have *all* found evidence of mass-asymmetric fission correlated with at least one of the same proton numbers $Z_{\text{FF}} = 36, 44$ associated with fission of ^{180}Hg [9, 10, 11, 12].

Three recent studies of heavy-ion induced fission of ^{178}Pt agree on the presence of mass-asymmetric fission [10, 13, 14]. However, they all disagree on the number of Gaussians required to fit the data, concluding there are one, two or three mass-asymmetric modes. This conflict may be due to different experimental conditions and fitting techniques, as well as varying fission statistics obtained.

A systematic approach to understand fission in the sub-actinide region is desirable. To achieve this, measurements along a line of N/Z may be beneficial. If we consider two nuclides with the same N/Z but different total A_{CN} , then a fission fragment

*Corresponding author

Email address: jacob.buete@anu.edu.au (J. Buete)

¹Permanent address: Variable Energy Cyclotron Centre, 1/AF, Bidhan Nagar, Kolkata 700064, India

²Present address: Image X Institute, University of Sydney, Central Clinical School, Sydney, Australia

³Present address: Australian Academy of Science, Ian Potter House, 9 Gordon Street, Acton, ACT 2601 Australia

Table 1: Beam-target combinations used to produce the compound nuclei (CN) in the present study. Centre-of-mass energies are corrected for energy loss through the half-target thickness. Excitation energies E_{gs}^* are given above the compound nucleus ground state. The quantity E_{sp}^* is the excitation energy above the saddle point of the l -dependent fission barrier [15].

Reaction	CN	Z_{CN}	$E_{c.m.}$ (MeV)	E_{gs}^* (MeV)	E_{sp}^* (MeV)
$^{32}\text{S} + ^{112}\text{Cd}$	^{144}Gd	64	114.6	69.8	38.0
$^{32}\text{S} + ^{116}\text{Sn}$	^{148}Dy	66	115.3	65.6	36.7
$^{32}\text{S} + ^{124}\text{Te}$	^{156}Er	68	117.4	65.1	37.1
$^{16}\text{O} + ^{144}\text{Sm}$	^{160}Yb	70	89.84	61.4	36.3
$^{32}\text{S} + ^{134}\text{Ba}$	^{166}Hf	72	119.4	58.3	35.3
$^{32}\text{S} + ^{142}\text{Ce}$	^{174}W	74	120.3	60.0	39.0
$^{32}\text{S} + ^{144}\text{Nd}$	^{176}Os	76	117.6	49.9	32.5
$^{34}\text{S} + ^{144}\text{Sm}$	^{178}Pt	78	117.6	37.7	23.8
$^{32}\text{S} + ^{152}\text{Sm}$	^{184}Pt	78	118.9	55.4	39.5
$^{32}\text{S} + ^{158}\text{Gd}$	^{190}Hg	80	119.4	54.1	40.4
$^{32}\text{S} + ^{164}\text{Dy}$	^{196}Pb	82	120.5	53.8	42.0
$^{32}\text{S} + ^{166}\text{Er}$	^{198}Po	84	120.6	45.1	35.7
$^{32}\text{S} + ^{172}\text{Yb}$	^{204}Rn	86	120.2	42.9	34.9
$^{32}\text{S} + ^{176}\text{Hf}$	^{208}Ra	88	125.1	42.8	36.4
$^{32}\text{S} + ^{180}\text{W}$	^{212}Th	90	128.9	41.1	36.1

produced by a particular shell-effect — forming the same proton or neutron number — should have the same total mass A_{FF} but appear at a *different* asymmetry. This moves systematically and predictably as A_{CN} is varied. Thus, examining the evolution of the fission mass distributions across a long chain of nuclides of similar N/Z can provide a consistent understanding of which, and how many, shell gaps are influencing fission.

In this Letter we present the first broad systematic measurement of fission mass distributions of neutron-deficient nuclei below the actinides. We show a detailed analysis of fission mass distributions of 14 nuclides ranging from ^{144}Gd ($Z = 64$) to ^{212}Th ($Z = 90$), populating every even- Z element.

2. Experiment

The measurements were performed at the Heavy-Ion Accelerator Facility at the Australian National University. Pulsed beams (FWHM ~ 1 ns) of $^{32,34}\text{S}$ and ^{16}O were delivered by the 14UD tandem electrostatic accelerator onto isotopically-enriched thin targets ranging from ^{112}Cd to ^{180}W , with areal densities from 7 to $140 \mu\text{g cm}^{-2}$. The targets were angled with their normals at 60° to the beam axis, with an incident beamspot size of ≤ 1 mm FWHM. Beam-target combinations are given in Table 1. Reactions were chosen to produce a series of neutron-deficient isotopes with restricted N/Z ratios between 1.28 – 1.39. The beam energies were chosen to minimise E^* whilst having sufficient fission cross-section to aim for 50 000 fissions per measurement. They resulted in excitation energies above the compound nucleus ground state E_{gs}^* of 41 – 70 MeV, as given in Table 1. Excitation energies above the fission saddle-point E_{sp}^* are most relevant, and estimates of these values are also given in Table 1. These are significantly lower, as a result of the height of the $l = 0$

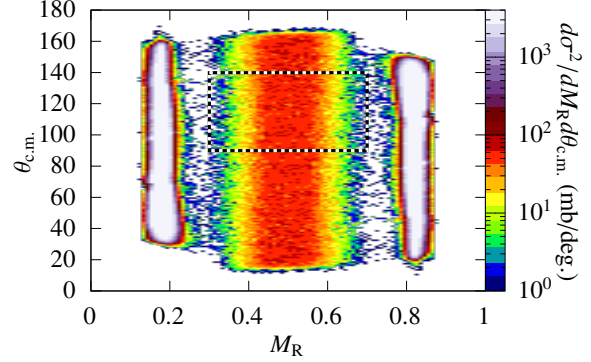


Figure 1: The mass-angle distribution for ^{176}Os . The vertical high intensity bands centred at $M_R = 0.18$ and 0.82 correspond to elastic and quasielastic scattering of the projectile and target nuclei. The central band corresponds to fissions. The black and white rectangle indicates the angular region used for fitting.

fission barrier and the rotational energy of the saddle-point configuration [15]. Details for estimating these values are provided in the supplementary material. Total fission statistics ranged between 38 000 and 174 000 events for each system.

Fission fragments were detected in coincidence in the CUBE fission spectrometer, with three position-sensitive multi-wire proportional counters (MWPC) configured as shown in Ref. [16]. The front $279 \times 357 \text{ mm}^2$ MWPC covered laboratory angles of 11° to 81° , while the back pair of detectors (one $279 \times 357 \text{ mm}^2$ and one $131 \times 357 \text{ mm}^2$) detected the complementary fission fragment between 52.6° and 168.6° .

Solid angle and cross-section normalization was achieved by simultaneous measurement in the MWPCs and two Si monitor detectors located at 22.5° [17] of sub-barrier elastic scattering of ^{58}Ni from a thin ^{197}Au target.

The mass-ratio of the fission fragments — defined as $M_R = m_1/(m_1 + m_2)$ — was determined by the kinematic coincidence method [18]. Corrections for the energy lost by the fragments in the target, backing, and detector windows were performed iteratively event-by-event using Ziegler’s energy loss systematics [19]. By using the measured M_R , instead of converting to atomic mass number, assumptions about pre-scission emission do not need to be made. An example of a mass-angle distribution is shown in Fig. 1 for ^{176}Os . Importantly, the mass-ratio centroids did not vary from 0.5 as a function of scattering angle $\theta_{c.m.}$, showing the absence of fast quasifission. A systematic classification based on fissility [17] suggests slow quasifission should be negligible except for the heaviest of these reactions [20, 21].

In order to avoid possible perturbations of the mass distributions at the detector edges, the results in this paper are presented for fission fragment scattering angles from $90^\circ < \theta_{c.m.} < 140^\circ$ (indicated by the black dashed box in Fig 1) where all reactions have full detector coverage as a function of mass-ratio. This cut reduces the statistical size used for analysis to between 21 000 and 96 000 fission events per measurement.

3. Results

3.1. Evidence for shell-driven fission

If the systems we have studied were to undergo fission only according to the classical liquid drop model, they would have mass distributions consistent with a single Gaussian centred at symmetry. Systematic deviations from a single Gaussian indicate the influence of quantum shells on the potential energy surface. Fig. 2 shows the measured fission mass-ratio distributions (without mirroring about $M_R = 0.5$) normalised to 100% yield. Some distributions ($Z_{CN} = 76, 78$) show clear mass-asymmetric peaks. To reveal the structure in all the distributions in the simplest way, first each was fitted with a single Gaussian (orange line). The deviations between the experiment and fit (residuals) are shown immediately to the right of each mass distribution.

For ^{178}Pt there is a large shell-driven component away from mass-symmetry, so the single Gaussian fit exceeds the experimental yield at symmetry, resulting in a negative residual. Compensating positive residuals appear away from symmetry, at the position of the shell-driven component. To guide the eye, consistently positive residuals are highlighted in pink, negative in blue. Every system shows residuals with clear structure. These are symmetric about $M_R = 0.5$, indicating their statistical significance. There is a clear systematic change in the structure of the residuals as Z_{CN} changes. This is discussed in detail below.

Beginning with ^{178}Pt (top right, Fig. 2), the double-peaked structure of the mass distribution is characteristic of a strong mass-asymmetric fission component. Previous analysis of this measurement [14] has shown ^{178}Pt to exhibit two different mass-asymmetric fission modes. The inner (most mass-symmetric) of these modes makes the largest contribution to the fission mass distribution, and is centred at $Z_{FF} = 35$ for the light fragment and $Z_{FF} = 43$ for the heavy fragment. No conclusion could be made in Ref. [14] as to which of the fragments determines the location of this mass-asymmetric fission mode.

If the light fragment with Z_{FF} near 35 were responsible, the positive residual structure (pink regions) should move towards mass-symmetry as the compound nucleus becomes lighter, occurring at symmetry for $Z_{CN} = 70$ (2×35). Indeed, the left column of residuals in Fig. 2 shows this is the case, with an excess of yield at mass-symmetry for $Z_{CN} = 72, 70, 68$. We note that the feature at mass-symmetry is both the strongest and narrowest for $Z = 68$ (2×34) and $Z = 72$ (2×36) among these systems. This may give insight into the strength of the pairing effects in driving fission. A dip at symmetry is re-established at $Z = 66, 64$ when a fission mode centred near $Z_{FF} = 35$ would again move away from symmetry.

If the heavy fragment (Z_{FF} near 43) were responsible, the positive residual structure should move towards symmetry with increasing Z_{CN} , reaching mass-symmetry near $Z_{CN} \approx 86$ (2×43). The rightmost column of Fig. 2 shows this *also* is the case, with peaks at symmetry for $Z = 86, 88, 90$. These results suggest that fission in this region is influenced by two distinct shell gaps, at different Z_{FF} , which coincide near Pt in both the heavy and light fragments. This is likely why the mass-asymmetric structure seen here for ^{176}Os , ^{178}Pt , and ^{190}Hg (as well as for ^{180}Hg [6]) is so pronounced.

This simple analysis enables us to uncover an important feature of the fission modes in this region. As Z_{CN} changes we observe the structure in the mass distributions correlated with the expected behaviour for a given Z_{FF} to show continuous movement towards, through, and away from mass-symmetry. Crucially, for Z_{CN} where the fission mode should appear at mass-symmetry we do observe a significant positive residual structure at symmetry. This leads to the conclusion that we should not think of shell effects as solely producing *mass-asymmetric* fission, but rather more generally of “shell-driven fission”, which may also appear at mass-symmetry dependent on the compound nucleus.

3.2. Identification of shell-effects

Non-Gaussian features in the measured mass spectra, that move characteristically across the mass spectrum as the compound nucleus changes, indicate the influence of one or more shell gaps in the single particle level spectrum of the fissioning system. The concept of a fission mode generally involves a bifurcation of trajectories on the potential energy surface (PES) which then lead to different valleys and to different scission configurations. The differing elongation of the system at the scission line of a valley associated with particular shell gaps should result in a defined variation to the total kinetic energy (TKE) for these trajectories.

Of course, the PES is not an experimental observable, so instead we take an empirical definition where a fission mode may be characterised by Gaussian distributions in both mass and relative kinetic energy defined by the shell gap (see Sec. 3.2.1); some number of which are required to fit the data. Examining the evolution of these ‘modes’ as part of a systematic comparison enables us to associate the independent evolution of a Gaussian mode (or identical evolution of multiple, correlated Gaussian modes) with the shell effects driving fission.

Increasing excitation energy complicates this picture as (i) the influence of shell effects is expected to wash out, and (ii) thermal fluctuations may take the fissioning system from one valley to another. However, as long as the influence of shell effects on the scission line remain — and thus impact the experimental observables of both mass and kinetic energy — the concept of a (Gaussian) fission mode as described above should remain a valid proxy for the influence of shell effects.

3.2.1. Two-dimensional fitting of M_R and RTKE

The qualitative evaluation of the residuals from a single-Gaussian fit to these fission mass distributions demonstrates that at least one shell-driven fission mode is present in all systems studied. Quantitative information on the number and location of these modes can be obtained by simultaneous fits to the mass-ratio and total kinetic energy distributions. Following the analysis described in Ref. [14], the expected dependence of the TKE on mass- and charge-split [22] was used to generate a mass-split dependent $\text{TKE}_{\text{Viola}}$, based on Viola’s TKE systematics [23]. Using this, we define $\text{RTKE} = \text{TKE}/\text{TKE}_{\text{Viola}}$ for each event. Then in the fitting process, each fission mode is represented as a two-dimensional Gaussian in both M_R and RTKE. Shell-driven

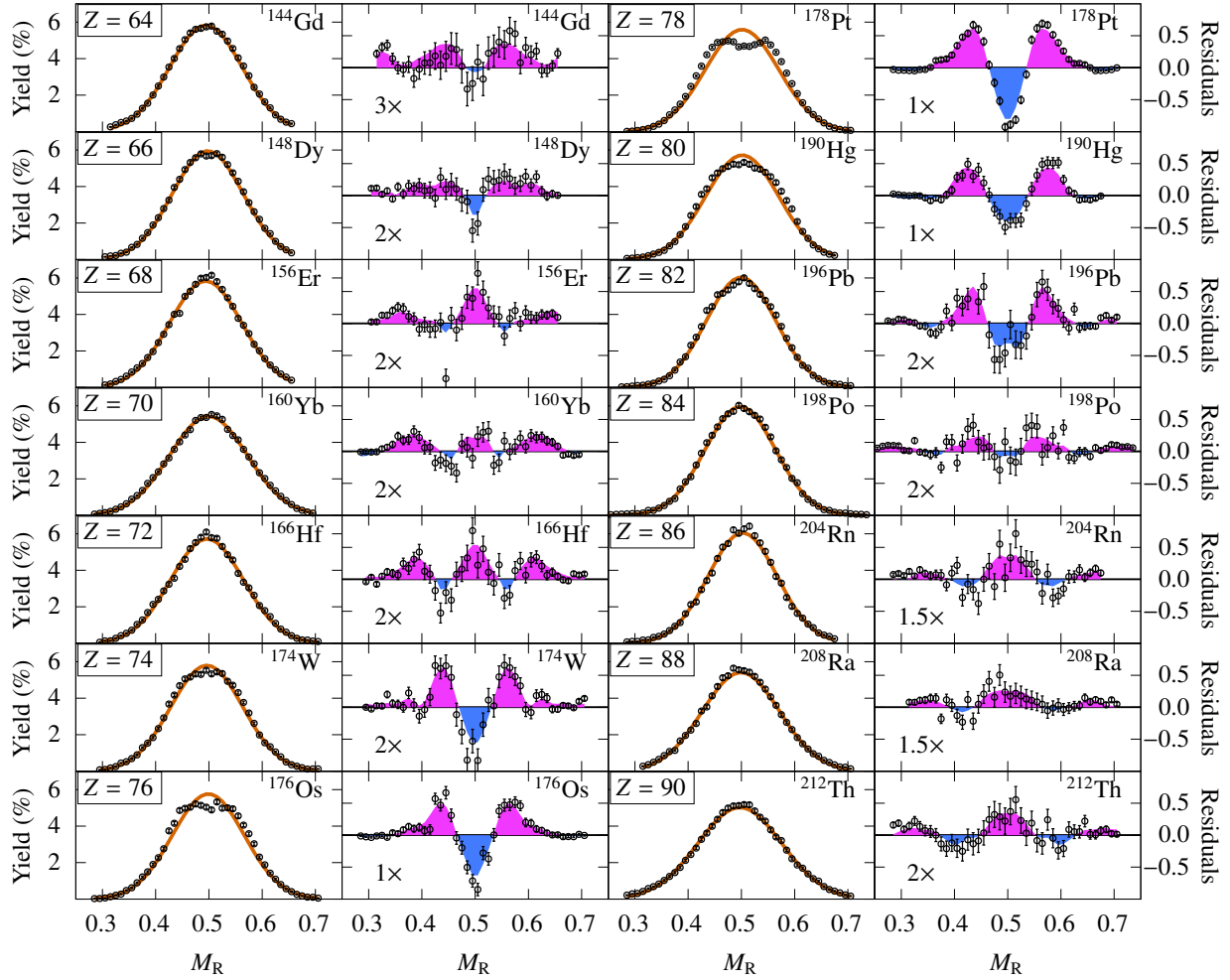


Figure 2: The fission fragment mass distributions for each compound nucleus of our systematic measurements ($N/Z = 1.24 - 1.39$). Each mass distribution (left panels) is shown together with a single Gaussian fit to the data (orange). The residuals from this fit (in units of yield in %) are shown in the panels immediately to the right of each distribution. The scaling factor (indicated in the bottom left of each panel) allows the residuals to share a common y-axis. To guide the eye, the residuals are highlighted in regions where they are consistently positive (pink) or negative (blue).

and liquid-drop fission modes can then be distinguished even at or near mass-symmetry, if they have significantly different RTKE.

The number of fission modes extracted in this fitting method is the *minimum* number required to provide a good fit to the two-dimensional data as assessed by the fit residuals. Using data collected using the same experimental conditions, having consistent resolution and similar statistics, and analysed with a consistent method, ensures that fitted results over the large range of systems can be compared reliably.

Small deviations in the measured fragment times-of-flight, due to beam pulse time-drift or \leq mm movement of the beam-spot on the target produce an RTKE distribution with a small linear dependence on M_R . Improving on the method of Ref. [14], an additional fit parameter was included to allow the two-dimensional Gaussian functions to tilt about $M_R = 0.5$. The maximum observed deviation from these effects represents a shift of less than 2 MeV ($\approx 1.3\%$) in the TKE at the extremes

of the mass-kinetic energy distribution. If the data were mirrored around symmetry as is common practice, this deviation would have resulted in broadening of the RTKE distributions and slightly poorer RTKE resolution at the extremes of the distributions, reducing the resolving power of the two-dimensional fitting process.

The fitting procedure was performed independently for each Z_{CN} , with no constraints on any fitted parameter. In all cases, the residual structure in the 2-D M_R -RTKE matrix revealed that *three* fission modes were sufficient to fit the data. These comprised one wide mass-symmetric mode (taken to be the liquid drop mode) and two shell-driven modes. From this point we denote the more mass-symmetric shell-driven mode as the "inner mode", and the more asymmetric mode as the "outer mode". The M_R projection and decomposition of the fit to each system can be found in the supplementary material.

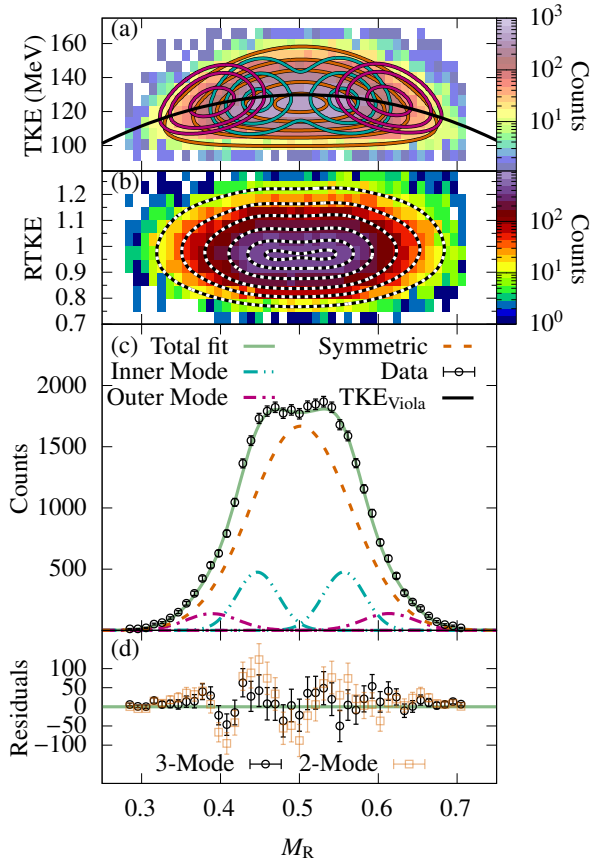


Figure 3: (colour online) Experimental results and best fit for ^{176}Os . Panel (a) shows the two-dimensional M_R -TKE distribution with overlaid contours representing each of the three fission modes fit to these data. Contour lines for the symmetric and inner shell-driven mode are at 10, 40, 100, and 220 counts, while the outer shell-driven mode contours indicate levels of 10, 25, and 40 counts. Panel (b) shows the derived M_R -RTKE distribution with the sum of the fitted modes shown in black dashed contour lines that indicate levels of 10, 40, 100, 220, 360, and 440 counts. Panel (c) shows the projection of the data onto M_R . The dashed and dot-dashed lines show the composition of the fit in terms of the liquid-drop symmetric and inner and outer shell-driven fission modes respectively. The residuals between the data and the total fit are shown in (d) along with the residuals (orange squares) from a fit comprising only one mass-asymmetric mode and one symmetric mode.

3.2.2. Example of fit to fission of ^{176}Os

An example of a two-dimensional fit is shown in Fig. 3 for ^{176}Os . In Fig. 3(a) the measured M_R -TKE distribution is shown with each of the three fission modes (fitted to M_R -RTKE) overlaid as contour lines. Each of the fission modes is found to be offset from the black line which indicates the value of $\text{TKE}_{\text{Viola}}$ after including the tilt in the data about $M_R = 0.5$. The symmetric fission mode (orange contours) is lower than $\text{TKE}_{\text{Viola}}$, as also reported for ^{178}Pt in Ref. [14]. This indicates that $\text{TKE}_{\text{Viola}}$ should not be used to predict the TKE of the liquid drop mode. Indeed, $\text{TKE}_{\text{Viola}}$ is an empirical estimate of the average TKE of the entire mass distribution, which may include more compact (higher kinetic energy) shell-driven fission modes. The average TKE of this measurement for ^{176}Os is $0.97 \text{ TKE}_{\text{Viola}}$.

In Fig. 3(b) the M_R -RTKE distribution is shown, together with

the best fit (black and white dashed contour lines) comprising the sum of the symmetric (liquid-drop) and two shell-driven fission modes. The projection of these data onto M_R in Fig. 3(c) demonstrates that the two-dimensional fit provides a good representation of the fission M_R distribution. 70% of the residuals in Fig. 3(d) (black circles) are within uncertainty of zero, consistent with the expectation for a statistical origin of the scatter. Fig. 3(d) also shows the residuals from a fit which contains a single shell-driven fission mode as well as the symmetric mode (orange squares). These show stronger deviations (consistent across $M_R = 0.5$) than the fit with two shell-driven modes. This — coupled with the need for a similar asymmetric mode in the nearby ^{178}Pt [14] — demonstrates the need for a second shell-driven fission mode in order to explain fully the structure of these data.

3.2.3. Extracting Proton and Neutron Shell Gaps

To extract the proton or neutron numbers associated with shell-driven fission, the centroids in M_R of the shell-driven modes were converted to proton and neutron numbers using the unchanged-charge distribution assumption (UCD) [26]. Here the charge-to-mass ratio of each of the fission products is assumed to be that of the compound nucleus. Alternative formulations for estimating the charge from the mass of the fission fragments exist — such as the minimum potential energy hypothesis (MPE) [27, 28] — which are better able to account for the observed UCD violation of actinide fission. However, recent measurements of UCD violation in the sublead region [29] show the opposite behaviour to that of the actinides (and the MPE) with the heavy fragment becoming less neutron-rich. The use of the MPE, or empirical estimates based on Ref. [29] would only change the determined centroid positions by less than 0.5 protons in all cases, which is below the precision we expect from this analysis. Thus, the UCD assumption is sufficient to determine the correlation of the fission modes with either proton or neutron number in the nascent fragments.

The deduced centroids of the inner shell-driven fission mode are shown in Fig. 4(a) and (b) for the proton and neutron numbers respectively, after conversion via the UCD. For each Z_{CN} (N_{CN}), centroids associated with the complementary light and heavy fragments are placed symmetrically around the diagonal (dashed) line which indicates the Z_{FF} (N_{FF}) of the fragment at mass-symmetry. The error bars represent the uncertainties from the fits. The coloured lines in each panel represent the values of known, or suggested, shell closures [3, 5, 24, 25].

Results from two previous heavy-ion fusion-fission measurements and analyses are also shown. Results for ^{180}Hg [8] are shown by grey pentagons, whilst the systematic measurements of Ref. [9] for systems from ^{176}Os to ^{220}Ra are indicated by grey crosses. The latter measured systems with a wide range of N/Z , which is useful in assessing the relative importance of proton and neutron shell gaps.

3.2.4. Do proton or neutron shells drive fission in this region?

The systems studied here mainly lie on a line of similar N/Z , so it is difficult to attribute unambiguously the origin of the shell-driven fission modes to proton rather than neutron shell

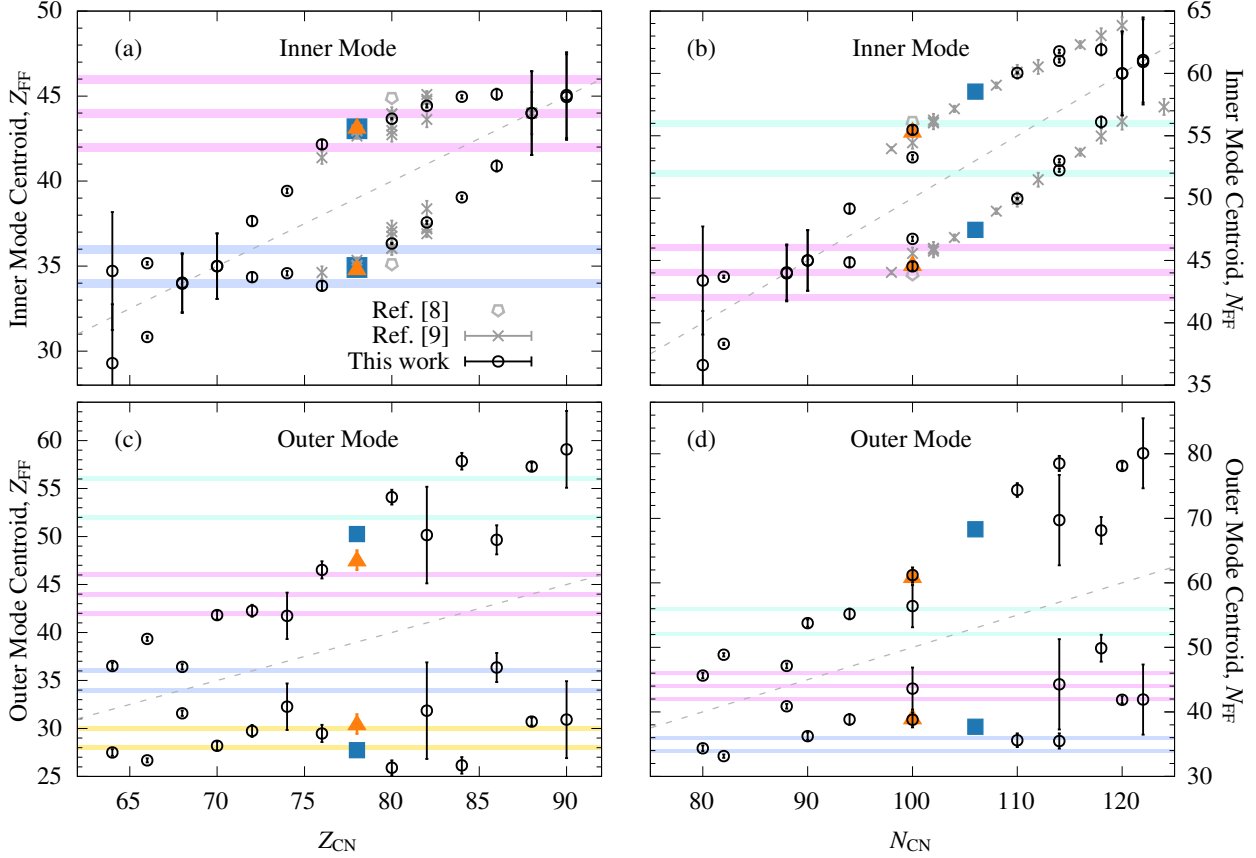


Figure 4: The proton Z (left) and neutron N (right) numbers for the shell-driven fission modes determined via a two-dimensional fit to the mass-RTKE distribution of each system, shown as a function of Z_{CN} and N_{CN} . Panels (a) and (b) show the centroids for the inner shell-driven fission mode, while (c) and (d) show the centroids for the outer shell-driven fission mode for the proton and neutron values respectively. Pt ($Z = 78$) has two points – the orange triangle corresponds to ^{178}Pt and the blue square is ^{184}Pt , uncertainties for these points are smaller than the marker size. Dashed diagonal lines at $Z = Z_{CN}/2$ and $N = N_{CN}/2$ show location of mass-symmetric fission to guide the eye. The coloured horizontal bands indicate the locations of known or suggested deformed shell closures that may affect fission [3, 5, 24, 25].

gaps. For example, Fig. 4(a) shows a correlation with proton number at $Z_{FF} \approx 34, 36$ up to $Z_{CN} = 80$, which is mirrored in Fig. 4(b) with $N_{FF} = 44$ for systems up to $N_{CN} = 100$. However, strong guidance can be obtained from a measurement of ^{184}Pt (not shown in Fig. 2, indicated by blue square points in Fig. 4). This can be compared with ^{178}Pt (orange triangular points), each having different N_{CN} ($N_{CN} = 100, 106$). Fits to ^{178}Pt and ^{184}Pt data return $Z_{FF} = 35$ for the inner shell-driven fission mode. However, N_{FF} moves from 44 to 47, parallel to the line of $N_{CN}/2$. Therefore, in the case of Pt we conclude that proton shell gaps are responsible for the inner shell-driven fission mode. The results of Ref. [9] (shown by grey crosses in the same figure) are consistent with this result, showing no evidence for any favoured N_{FF} above $N_{CN} = 98$. Measurements for different isotopes of lighter elements would be necessary to determine whether any neutron shell gap near $N_{FF} = 44$ might be playing a role.

3.2.5. Systematics of the Inner Mode

Beginning with ^{144}Gd and ^{148}Dy ($Z_{CN} = 64, 66$) in Fig. 4(a) the inner mode is located near $Z_{FF} = 34, 36$, in the heavy fragment. With increasing Z_{CN} the inner mode remains between $Z_{FF} = 34, 36$, coinciding with the line of mass-symmetry for

$Z_{CN} = 68, 70$ and continuing in the light fragment until Hg ($Z_{CN} = 80$) is reached. As Z_{CN} increases towards $Z_{CN} = 90$, the heavy fragment shows a strong correlation with $Z_{FF} = 44, 46$; the light fragment increases in Z_{FF} to compensate. For the heaviest two nuclei studied (Ra and Th) we again observe the inner fission mode to coincide with the line indicating mass-symmetry.

3.2.6. Systematics of the Outer Mode

The shell gap(s) responsible for the outer shell-driven fission mode could not be conclusively determined from this measurement, due in large part to the significant statistical limitations imposed by the low yields at large mass asymmetries. Despite these limitations there is some structure in the evolution of the centroids of this outer mode, shown in Fig. 4(c) and (d) with both increasing Z_{CN} and N_{CN} . The initial impression is that the light fragment is correlated with proton numbers near $Z = 28, 30$ ($N = 34, 36$) for all systems, with the complementary fragment increasing in mass to compensate with increasing Z_{CN} (N_{CN}). This would indicate the possibility of a single fission mode responsible for the light fragment of the outer shell-driven mode for many systems over this region.

However, it can be also seen in Fig. 4(c) that in several cases

the Z_{FF} of the outer fission mode appears to be correlated with the same shell gaps that drive the inner mode. In particular, the outer mode produces fission fragments at $Z_{\text{FF}} = 36$ for isotopes of Gd, Er, Rn ($Z_{\text{CN}} = 64, 68, 86$), and is correlated with $Z_{\text{FF}} = 42$ for Yb, Hf, and W ($Z_{\text{CN}} = 70 - 74$). Given the significant scatter observed for the outer mode in the heaviest systems ($Z_{\text{CN}} \geq 86$) we can also not rule out a contribution from shell gaps associated with Standard I and II fission. Larger measurement sizes in future, focussed on these regions, are needed to fully elucidate the nature of the shells driving this very asymmetric fission mode in future.

3.2.7. Comparison of qualitative and quantitative analysis

The results shown in Fig. 4(a) are able to explain many of the features seen in the residuals from the single Gaussian fits in Fig. 2. The large mass-asymmetric positive residuals in Fig. 2 for Os, Pt, and Hg ($Z_{\text{CN}} = 76, 78, 80$) may be partially attributed to the overlap of two deformed shell-effects in complementary fission fragments: the inner mass-asymmetric mode of ^{178}Pt produces fragments with the light fragment near $Z_{\text{FF}} = 34, 36$ and the heavy fragment near $Z_{\text{FF}} = 44$. Furthermore, systems that show a significant positive residual structure at mass-symmetry in Fig. 2, also produce a fit with their inner fission mode at symmetry. These modes agree with the deformed shell effects now seen to drive the inner fission mode with changing Z_{CN} .

Thus, the qualitative analysis of the residuals from a single Gaussian has been successful in identifying the existence and rough location of shell-driven fission modes. However, the residuals are not a good source of information on other quantities, such as the strength or yield of the shell-driven modes. The limitations on what can be determined from the combination of residuals and excitation energy E_{sp}^* are discussed in detail in the supplementary material.

4. Conclusions

The combination of large measurement sizes and consistent application of new analysis techniques has revealed the need for at least two shell-driven fission modes in all systems measured between $Z_{\text{CN}} = 64 - 90$, including one at large mass-asymmetry. This agrees with the conclusions of past works which suggest the possibility of multi-modal mass-asymmetric fission in ^{178}Pt and ^{190}Hg [11, 10, 14], but extends it to the entire range studied here. The systematic measurement of all even- Z compound nuclei in this range allows us to track the evolution of the shell-driven fission modes extracted from the fits to experimental data. A systematic trend is seen for all three fission modes. One is mass-symmetric and wide, with similar width in M_{R} for all systems. According to the interpretation of actinide fission modes [2] this would be identified with the liquid drop mode. The two others are narrower, and their systematically changing location in M_{R} as Z_{CN} varies is consistent with different proton shell gaps being responsible. It is thus concluded that these are separate shell effects, reflecting the existence of discrete structures in the PES, either influencing the shape of a valley, or even producing new ones.

The proton and neutron number of the fission fragments was determined under the UCD assumption. Previous observations have indicated that UCD is violated for fission of the actinides [26] where the heavy fragment is 1.6% more neutron-rich than the compound nucleus and in ^{178}Hg [29] where the light fragment is seen to be 2.4% more neutron-rich. Given the manner of the UCD violation changes and that the degree of violation seen in either case would only modify the determined proton Z_{FF} at most ± 0.5 this would not alter our conclusions about the shell effects driving fission in this region.

Starting at $Z_{\text{CN}} = 64$, the shell-driven fission mode associated with $Z_{\text{FF}} = 34, 36$ initially produces the observed heavy fragment peak, then for higher Z_{CN} up to Pt ($Z_{\text{CN}} = 78$) the light fragment peak. Importantly, the experimental data shows the influence of this mode as it passes through mass-symmetry at $Z_{\text{CN}} = 68 - 72$. With increasing Z_{CN} both the data and fits show a smooth transition from domination by the $Z_{\text{FF}} = 34, 36$ shell gap to $Z_{\text{FF}} = 44, 46$, including a region of simultaneous population in ^{176}Os , $^{178,184}\text{Pt}$ and ^{190}Hg . This may well explain the significant enhancement of the asymmetric fission yields seen for these systems [10, 14] as well as for ^{180}Hg [6]. The experimental data are also consistent with the $Z_{\text{FF}} = 44, 46$ fission mode moving towards mass-symmetry as Z_{CN} approaches $2 \times Z_{\text{FF}}$. Further measurements for heavier actinides will be needed to determine if this mode continues in the light fragment beyond $Z_{\text{CN}} = 90$.

Measurements of fission characteristics along a line of similar N/Z over a wide range of Z_{CN} provide an excellent tool to examine the evolution of shell-driven fission. Interestingly, the qualitative systematic behaviour of structure in the residuals of single-Gaussian fits to the fission mass distributions revealed many of the same conclusions as from our two-dimensional fitting. The former approach may be useful for systematic measurements where kinetic energy has not been measured or the measurement sizes are insufficient for the multi-parameter two-dimensional fitting analysis we have introduced. Once the major shell effects have been identified, targeted measurements of their evolution along isotopic chains (crossing lines of constant N/Z) can disambiguate the role of protons and neutrons in driving the fission modes.

5. Acknowledgements

The authors acknowledge support from the Australian Research Council through Discovery Grants No. DP190100256, No. DP190101442, No. DP200100601, No. DP230101028, and No. DE230100197. Support for the Heavy Ion Accelerator Facility operations from the Australian National Collaborative Research Infrastructure (NCRIS) HIA project is acknowledged. We thank M.A. Stoyer for his contribution towards running the experiment.

References

- [1] Lise Meitner and O. R. Frisch. Disintegration of Uranium by Neutrons: A New Type of Nuclear Reaction. *Nature*, 143(3615):239–240, February 1939.
- [2] Ulrich Broosa, Siegfried Grossmann, and Andreas Müller. Nuclear scission. *Physics Reports*, 197(4):167–262, December 1990.

- [3] C. Böckstiegel, S. Steinhäuser, K. H. Schmidt, H. G. Clerc, A. Grewe, A. Heinz, M. de Jong, A. R. Jungmans, J. Müller, and B. Voss. Nuclear-fission studies with relativistic secondary beams: Analysis of fission channels. *Nuclear Physics A*, 802(1):12–25, April 2008.
- [4] K. H. Schmidt, S. Steinhäuser, C. Böckstiegel, A. Grewe, A. Heinz, A. R. Jungmans, J. Benlliure, H. G. Clerc, M. de Jong, J. Müller, M. Pfützner, and B. Voss. Relativistic radioactive beams: A new access to nuclear-fission studies. *Nuclear Physics A*, 665(3):221–267, February 2000.
- [5] Guillaume Scamps and Cédric Simenel. Impact of pear-shaped fission fragments on mass-asymmetric fission in actinides. *Nature*, 564(7736):382–385, December 2018.
- [6] A. N. Andreyev, J. Elseviers, M. Huyse, P. Van Duppen, S. Antalic, A. Barzakh, N. Bree, T. E. Cocolios, V. F. Comas, J. Diriken, D. Fedorov, V. Fedosseev, S. Franchoo, J. A. Heredia, O. Ivanov, U. Köster, B. A. Marsh, K. Nishio, R. D. Page, N. Patronis, M. Seliverstov, I. Tsekhanovich, P. Van den Bergh, J. Van De Walle, M. Venhart, S. Vermote, M. Veselsky, C. Wagemans, T. Ichikawa, A. Iwamoto, P. Möller, and A. J. Sierk. New Type of Asymmetric Fission in Proton-Rich Nuclei. *Physical Review Letters*, 105(25):252502, December 2010.
- [7] E. Prasad, D. J. Hinde, K. Ramachandran, E. Williams, M. Dasgupta, I. P. Carter, K. J. Cook, D. Y. Jeung, D. H. Luong, S. McNeil, C. S. Palshetkar, D. C. Rafferty, C. Simenel, A. Wakhle, J. Khuyagbaatar, Ch. E. Düllmann, B. Lommel, and B. Kindler. Observation of mass-asymmetric fission of mercury nuclei in heavy ion fusion. *Physical Review C*, 91(6):064605, June 2015.
- [8] K. Nishio, A. N. Andreyev, R. Chapman, X. Derckx, Ch. E. Düllmann, L. Ghys, F. P. Heßberger, K. Hirose, H. Ikezoe, J. Khuyagbaatar, B. Kindler, B. Lommel, H. Makii, I. Nishinaka, T. Ohtsuki, S. D. Pain, R. Sagaidak, I. Tsekhanovich, M. Venhart, Y. Wakabayashi, and S. Yan. Excitation energy dependence of fragment-mass distributions from fission of $^{180,190}\text{Hg}$ formed in fusion reactions of $^{36}\text{Ar} + ^{144,154}\text{Sm}$. *Physics Letters B*, 748:89–94, September 2015.
- [9] E. Prasad, D. J. Hinde, M. Dasgupta, D. Y. Jeung, A. C. Berriman, B. M. A. Swinton-Bland, C. Simenel, E. C. Simpson, R. Bernard, E. Williams, K. J. Cook, D. C. Rafferty, C. Sengupta, J. F. Smith, K. Vo-Phuoc, and J. Walshe. Systematics of the mass-asymmetric fission of excited nuclei from ^{176}Os to ^{206}Pb . *Physics Letters B*, 811:135941, December 2020.
- [10] E. M. Kozulin, G. N. Knyazheva, I. M. Itkis, M. G. Itkis, Y. S. Mukhamejanov, A. A. Bogachev, K. V. Novikov, V. V. Kirakosyan, D. Kumar, T. Banerjee, M. Cheralu, M. Maiti, R. Prajapat, R. Kumar, G. Sarkar, W. H. Trzaska, A. N. Andreyev, I. M. Harca, A. Mitu, and E. Vardaci. Fission of $^{180,182,183}\text{Hg}^*$ and $^{178}\text{Pt}^*$ nuclei at intermediate excitation energies. *Physical Review C*, 105(1):014607, January 2022.
- [11] A. A. Bogachev, E. M. Kozulin, G. N. Knyazheva, I. M. Itkis, M. G. Itkis, K. V. Novikov, D. Kumar, T. Banerjee, I. N. Diatlov, M. Cheralu, V. V. Kirakosyan, Y. S. Mukhamejanov, A. N. Pan, I. V. Pchelintsev, R. S. Tikhomirov, I. V. Vorobiev, M. Maiti, R. Prajapat, R. Kumar, G. Sarkar, W. H. Trzaska, A. N. Andreyev, I. M. Harca, and E. Vardaci. Asymmetric and symmetric fission of excited nuclei of $^{180,190}\text{Hg}$ and $^{184,192,202}\text{Pb}$ formed in the reactions with ^{36}Ar and $^{40,48}\text{Ca}$ ions. *Physical Review C*, 104(2):024623, August 2021.
- [12] B. M. A. Swinton-Bland, M. A. Stoyer, A. C. Berriman, D. J. Hinde, C. Simenel, J. Buete, T. Tanaka, K. Banerjee, L. T. Bezzina, I. P. Carter, K. J. Cook, M. Dasgupta, D. Y. Jeung, C. Sengupta, E. C. Simpson, and K. Vo-Phuoc. Mass-asymmetric fission of $^{205,207,209}\text{Bi}$ at energies close to the fission barrier using proton bombardment of $^{204,206,208}\text{Pb}$. *Physical Review C*, 102(5):054611, November 2020.
- [13] I. Tsekhanovich, A. N. Andreyev, K. Nishio, D. Denis-Petit, K. Hirose, H. Makii, Z. Matheson, K. Morimoto, K. Morita, W. Nazarewicz, R. Orlandi, J. Sadhukhan, T. Tanaka, M. Vermeulen, and M. Warda. Observation of the competing fission modes in ^{178}Pt . *Physics Letters B*, 790:583–588, March 2019.
- [14] B. M. A. Swinton-Bland, J. Buete, D. J. Hinde, M. Dasgupta, T. Tanaka, A. C. Berriman, D. Y. Jeung, K. Banerjee, L. T. Bezzina, I. P. Carter, K. J. Cook, C. Sengupta, C. Simenel, E. C. Simpson, and M. A. Stoyer. Multimodal mass-asymmetric fission of ^{178}Pt from simultaneous mass-kinetic energy fitting. *Physics Letters B*, 837:137655, February 2023.
- [15] Arnold J. Sierk. Macroscopic model of rotating nuclei. *Physical Review C*, 33(6):2039–2053, June 1986.
- [16] T. Banerjee, D. J. Hinde, D. Y. Jeung, K. Banerjee, M. Dasgupta, A. C. Berriman, L. T. Bezzina, H. M. Albers, Ch. E. Düllmann, J. Khuyagbaatar, B. Kindler, B. Lommel, E. C. Simpson, C. Sengupta, B. M. A. Swinton-Bland, T. Tanaka, A. Yakushev, K. Eberhardt, C. Mokry, J. Runke, P. Thörle-Pospiech, and N. Trautmann. Systematic evidence for quasifission in ^9Be -, ^{12}C -, and ^{16}O -induced reactions forming $^{258,260}\text{No}$. *Physical Review C*, 102(2):024603, August 2020.
- [17] R. du Rietz, E. Williams, D. J. Hinde, M. Dasgupta, M. Evers, C. J. Lin, D. H. Luong, C. Simenel, and A. Wakhle. Mapping quasifission characteristics and timescales in heavy element formation reactions. *Physical Review C*, 88(5):054618, November 2013.
- [18] D. J. Hinde, M. Dasgupta, J. R. Leigh, J. C. Mein, C. R. Morton, J. O. Newton, and H. Timmers. Conclusive evidence for the influence of nuclear orientation on quasifission. *Physical Review C*, 53(3):1290–1300, March 1996.
- [19] James F. Ziegler and Jochen P. Biersack. The Stopping and Range of Ions in Matter. In D. Allan Bromley, editor, *Treatise on Heavy-Ion Science: Volume 6: Astrophysics, Chemistry, and Condensed Matter*, pages 93–129. Springer US, Boston, MA, 1985.
- [20] A. C. Berriman, D. J. Hinde, M. Dasgupta, C. R. Morton, R. D. Butt, and J. O. Newton. Unexpected inhibition of fusion in nucleus–nucleus collisions. *Nature*, 413(6852):144–147, September 2001.
- [21] L. T. Bezzina, E. C. Simpson, D. J. Hinde, and M. Dasgupta. Observation of suppression of heavy-ion fusion by slow quasifission. *EPJ Web of Conferences*, 306:01029, 2024.
- [22] D. J. Hinde, D. Hilscher, H. Rossner, B. Gebauer, M. Lehmann, and M. Wilpert. Neutron emission as a probe of fusion-fission and quasifission dynamics. *Physical Review C*, 45(3):1229–1259, March 1992.
- [23] V. E. Viola, K. Kwiatkowski, and M. Walker. Systematics of fission fragment total kinetic energy release. *Physical Review C*, 31(4):1550–1552, April 1985.
- [24] A. O. Macchiavelli, J. Burde, R. M. Diamond, C. W. Beausang, M. A. Deleplanque, R. J. McDonald, F. S. Stephens, and J. E. Draper. Superdeformation in $^{104,105}\text{Pd}$. *Physical Review C*, 38(2):1088–1091, August 1988.
- [25] Guillaume Scamps and Cédric Simenel. Effect of shell structure on the fission of sub-lead nuclei. *Physical Review C*, 100(4):041602, October 2019.
- [26] A. C. Wahl, R. L. Ferguson, D. R. Nethaway, D. E. Troutner, and K. Wolfsberg. Nuclear-Charge Distribution in Low-Energy Fission. *Physical Review*, 126(3):1112–1127, May 1962.
- [27] H. M. Blann. *Fission of Gold with 112-MeV C12 Ions: A Yield-Mass and Charge-Distribution Study*. PhD thesis, Lawrence Radiation Laboratory, University of California, Berkeley, California, May 1960.
- [28] Charles D. Coryell, Morton Kaplan, and Richard D. Fink. Search for Correlations of Most Probable Nuclear Charge z_p of Primary Fission Fragments with Composition and Excitation Energy. *Canadian Journal of Chemistry*, 39(3):646–663, March 1961.
- [29] C. Schmitt, A. Lemasson, K.-H. Schmidt, A. Jhingan, S. Biswas, Y. H. Kim, D. Ramos, A. N. Andreyev, D. Curien, M. Ciemala, E. Clément, O. Dorvaux, B. De Canditiis, F. Didierjean, G. Duchêne, J. Dudouet, J. Frankland, B. Jacquot, C. Raison, D. Ralet, B.-M. Retailleau, L. Stuttgé, and I. Tsekhanovich. Experimental Evidence for Common Driving Effects in Low-Energy Fission from Sublead to Actinides. *Physical Review Letters*, 126(13):132502, April 2021.

Supplementary Material for Universality of Shell Effects in Fusion-Fission Mass Distributions

J. Buete^{a,*}, B. M. A. Swinton-Bland^{a,3}, D. J. Hinde^a, K. J. Cook^{a,b}, M. Dasgupta^a, A. C. Berriman^a, D. Y. Jeung^a, K. Banerjee^{a,1}, L. T. Bezzina^a, I. P. Carter^a, C. Sengupta^{a,2}, C. Simenel^{a,c}, E. C. Simpson^a

^aDepartment of Nuclear Physics and Accelerator Applications, Research School of Physics, Australian National University, Canberra, ACT 2601, Australia

^bFacility for Rare Isotope Beams, Michigan State University, Michigan 48824, USA

^cDepartment of Fundamental and Theoretical Physics, Research School of Physics, Australian National University, Canberra, ACT 2601, Australia

Keywords: heavy-ion induced fission, fission, nuclear reactions, fission mass distributions, sub-lead fission, shell-driven fission

1. Excitation Energy

1.1. Mean Excitation Energy above the Saddle Point

Table 1 of the Letter gives values for the mean excitation energy above the saddle point configuration E_{sp}^* for each reaction. To estimate this, the first step was to calculate the FRLDM l -dependent barrier and the rotational energy of the ground-state configuration using BARFIT [1]. The ground state excitation energy E_{gs}^* is then used with these values to determine the net excitation energy above the saddle point for each partial wave l . The l distribution of each fusion reaction was calculated using CCFULL [2]. The estimated mean E_{gs}^* for each reaction was then evaluated from the weighted mean of the E_{gs}^* for each l -value.

For the heavier systems, having high fissility, most fusion will lead to fission, so an average over the fusion partial waves is an appropriate estimate of E_{sp}^* . However, for the lighter systems in our measurement, only the highest l -values result in fission. The l distributions for fission events cannot currently be reliably estimated in the absence of experimental cross-section data. Thus, the average E_{sp}^* for these systems will in reality be lower than the values given in Table 1.

2. Magnitude of single Gaussian fit residuals

A major contributor to the size of the residual structure appears to be “geometric” in origin, depending strongly on the location of the shell-driven Gaussian modes and their widths relative to the liquid drop mode.

¹⁷⁶Os, ¹⁷⁸Pt and ¹⁹⁰Hg may well result in the largest residual structure because the shell gaps for these systems drive mass-asymmetric fission far enough from symmetry to result in flat-topped or double-peaked experimental distributions. This shape

of distribution is particularly poorly approximated by a single Gaussian and therefore results in a large residual amplitude.

In contrast, if a shell mode were located at mass-symmetry, like the liquid drop mode, then, depending on the relative widths of the two Gaussian modes, the residuals could be small, even if the weight of the shell mode were large.

A further potential contributor to the magnitude of the residuals is differences in the strength of the outer mass-asymmetric mode. This should affect the width of the single Gaussian fit, and therefore change the magnitude of the residuals closer to mass-symmetry.

The effect of E_{sp}^* on the size of the residual deviations can be tested among systems close to each other in Z . Consider the results for the compound nuclei ¹⁷⁸Pt and ¹⁹⁰Hg. As seen in Fig. 2 in the Letter, the residuals from the single Gaussian fits are not very different, although their mean excitation energies E_{sp}^* in Table 1 differ by 16.4 MeV. This suggests that the damping of the observed effects of shell structure with excitation energy is not very rapid. Making this comparison for the *same* system measured at different bombarding energies would be a good test of the rate of shell damping with E_{sp}^* .

Throughout the data set, using the estimates of E_{sp}^* from Table 1 and the scale of the residual structure from a single Gaussian fit shown in Fig. 2 of the Letter, we find no consistent relationship between the size of the residuals and the excitation energy. Indeed, comparing ¹⁹⁰Hg to ¹⁴⁴Gd we see a reduction by a factor of three in the scale of the residual structure with a 2.4 MeV *decrease* in E_{sp}^* .

In summary, although the location of structure in the residuals appears to give useful information for the location of shell gaps, the size of the residuals for quite different fissioning nuclides is generally too sensitive to other variables to give reliable information on the relative strengths of shell effects.

3. Multi-Gaussian fit results

The M_R spectra resulting from the 2-D fits to each system, including their decomposition into a symmetric liquid drop and two shell-driven fission modes, are shown here in Fig. 1.

*Corresponding author

Email address: jacob.buete@anu.edu.au (J. Buete)

¹Permanent address: Variable Energy Cyclotron Centre, 1/AF, Bidhan Nagar, Kolkata 700064, India

²Present address: Image X Institute, University of Sydney, Central Clinical School, Sydney, Australia

³Present address: Australian Academy of Science, Ian Potter House, 9 Gordon Street, Acton, ACT 2601 Australia

We note that there is a significant overlap of the fission mode Gaussians in all measured systems. This results in fits in which the yields and widths of each fission mode become highly correlated. Thus, the fitted yields become unreliable [3]. In contrast, the *centroids* of the shell-driven modes generally have much smaller uncertainties, as shown in Fig.4 of the Letter.

For this reason, the decomposition of the fits into the individual fission modes demonstrates an inconsistent evolution of the yields of each mode despite the observed smooth evolution in the location of the inner shell-driven mode in the Letter. To illustrate this, for $^{178, 184}\text{Pt}$ the fitted model gives identical proton numbers for the inner shell-driven mode but differ by a factor of four in the ratio of the yield of this mode compared to the symmetric fission mode.

References

- [1] Arnold J. Sierk. Macroscopic model of rotating nuclei. *Physical Review C*, 33(6):2039–2053, June 1986.
- [2] K. Hagino, N. Rowley, and A. T. Kruppa. A program for coupled-channel calculations with all order couplings for heavy-ion fusion reactions. *Computer Physics Communications*, 123(1):143–152, December 1999.
- [3] J. Buete. *Impact of Shell Structure on Fusion and Fission*. PhD thesis, The Australian National University, Canberra, Australia, 2023.

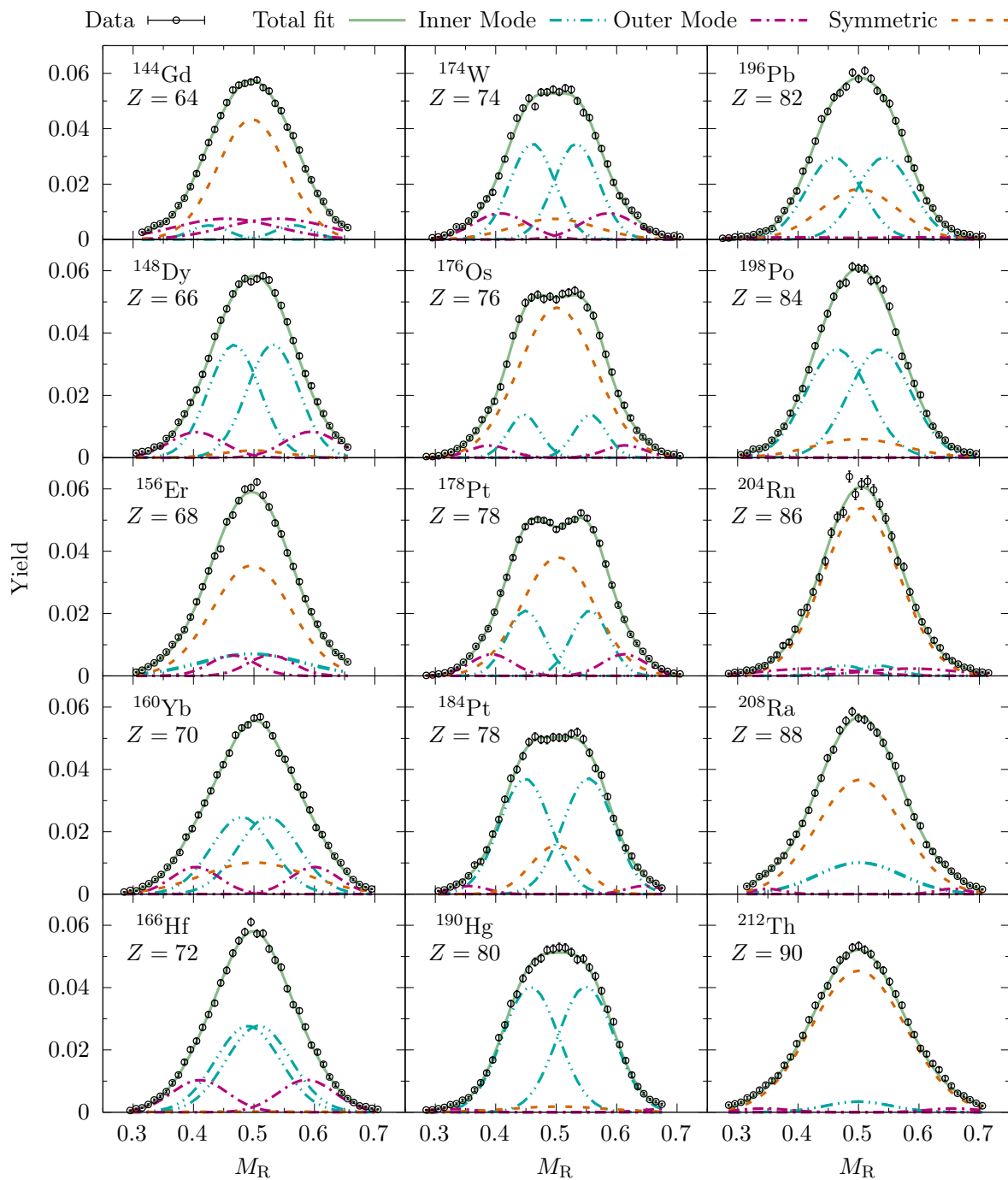


Figure 1: The decomposition of the fits shown in Fig. 4 in the main letter.